Structural evolution of HMX during processing operations

Mathieu Guerain, Pascal Palmas, Alexandre Lecardeur

Structural evolution of HMX during processing operations

Mathieu Guerain[1], Pascal Palmas[2], Alexandre Lecardeur[2]*

[1]Université de Lille, CNRS, INRAE, Centrale Lille, UMR 8207- UMET - Unité Matériaux et Transformations, F-59000 Lille, France

[2]CEA DAM le Ripault, F-37260 Monts, France.

*mathieu.guerain@univ-lille.fr

Abstract

The impact of processing operations such as chemical synthesis conditions, milling, coating and pressing operations on the crystallographic structure of HMX has been studied using X-ray diffraction and Rietveld analysis. Strong differences in grain morphology and X-ray patterns were first observed after synthesis on two different setups with different washing methods. Diffraction pattern refinements were tentatively performed on the basis of known structures and assuming preferential orientations. The impossibility of achieving satisfactory agreement, even considering the orientation of several planes, could be attributed to the presence of polymorphism or hydrates. The possible new polymorphs or hydrates were metastable since milling led to the stable ß-HMX polymorph. No such transformation occurred during the coating operation, but an increase in structural defects was observed. Finally, the pressing step did not induce any transformation but surprisingly led to a decrease in structural defects, probably due to isotropic deformation of the crystallographic cell and the repairing effect of the associated thermal treatment.

1. Introduction

HMX (octahydro-1,3,5,7-tetranitro-1,3,5,7-tetrazocine, $C_4H_8N_8O_8$) is a commonly used organic explosive having a high detonation velocity (9100 m/s) and a high detonation pressure (39 300MPa). It is well known that the intrinsic properties of such energetic materials are closely related to their crystalline structure, i.e. the relative spatial arrangements of the molecules, and thus the polymorphic phase of the compound considered[1]. In some cases, especially at the synthesis step, solvatomorphism issue may be encountered. Solvatomorphism is close to polymorphism. The crystal structures of the substance are defined by different unit cells but these unit cells differ in their elemental composition through the inclusion of one or more molecules of solvent (water for example)[2].

HMX has a rich polymorphism with six known polymorphs reported in the literature. The stable form at ambient temperature is ß-HMX[3,4]. The crystal structure of ß-HMX is well documented[4]. A view of the crystallographic cell of β-HMX is given in Figure 1. It is a monoclinic crystal, space group $P2_1/c$ with the following lattice parameters: a=6.540 Å, b=11.050 Å, c=8.700 Å, and *ß* = 124.30°. The cell volume is equal to 519.387 $Å^3$. In ß-HMX, the molecules assemble together by hydrogen bonding with two molecules per cell in a chair conformation, stacking along the c axis. This form is stable between -150°C and 103°C. Then, it is transformed into α-HMX, an orthorhombic phase, between 103°C and 162°C[3]. The δ-HMX[5] form is obtained above 160°C. This phase is hexagonal. The fourth form γ–HMX is

monoclinic. It has been observed by some authors around 160°C[6,7] between the α→δ transition. The melting of the compound occurs around 280°C. The ζ-HMX and ε-HMX forms exist under high pressure at ambient temperature. They appear respectively at 6.2 and 12.6 GPa[8]. HMX has also numerous solvates or cocrystals. Ten crystallographic structures of hydrates, solvates or cocrystals of HMX where identified after a research in the crystallographic databases (Cambridge structural Database, Crystallography Open Database)[9–12] .

The interest of studying polymorphism is twofold: i) in some cases, the synthesis of new polymorphic forms, hydrates or solvates makes it possible to detect and select new forms having better properties than the form usually used; ii) conversely, unwanted polymorphic transformations can occur during manufacturing processes and potentially degrade material performances. To evaluate the existence and the number of polymorphs that an explosive can present, recrystallization in different solvents is very often studied. For example, β-RDX was obtained in 1950 by crystallization from high boiling solvents such as nitrobenzene[13] and differs from stable α-RDX determined by Choi et al.[14]. The example of CL-20 is particularly relevant. Indeed, CL-20 has been recrystallized in more than 20 different solvents. It leads to generate multiple polymorphs or mixtures of polymorphs of CL-20 depending on the experimental conditions[15–17]. CL-20 is also known[18], as well as DAAF[19]to have solvate forms. It shows that the mode of crystallization has a significant impact on the polymorphic form obtained.

In addition to polymorphic transformations, the same form can also experience crystallographic modifications such as the appearance of crystalline defects or a slight change in crystal lattice parameters[20,21] that can also have consequences on material properties. The two parameters representing structural defects of the material are crystallite size and microstrain[22]. The crystallite size L, or coherent diffraction domain, is the size of the perfect crystal. It can be viewed as an average length between two structural defects in a given plane family. The microstrain ε corresponds to lattice distortions due to slight displacements of atoms and molecules from their position in an ideal crystal. In all cases, an analogy can be made with the many works published in the field of pharmaceutical applications. These works show that different processes can affect the crystallographic structure of a molecular material, influencing the final properties of the compound[23,24].

In the present article, we have investigated the effect of changing chemical synthesis setup and washing conditions as well as milling, coating and pressing processes on the crystallographic structure of HMX. Morphological analyses were carried out using optical microscopy. X-ray diffraction was used at each step of the process to reveal any slight changes in the crystallographic structure of the material. Indeed, each polymorph or solvate of HMX exhibits a different X-ray pattern, because peak positions are related to the lattice parameter and peak intensities are related to the position of atoms (and consequently molecules) in the cell.

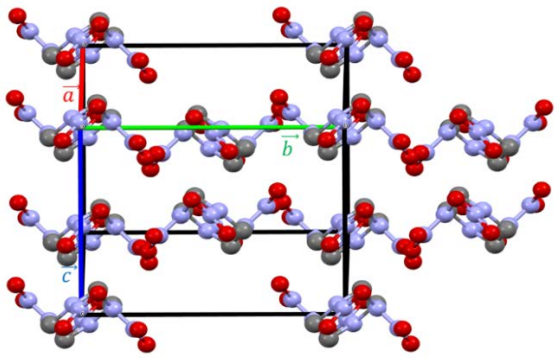

Figure 1: View along the $\vec{c}$ axis of the ß-HMX structure (top). C atoms are black, N atoms are blue, O atoms are red, H atoms are not indicated.

2. Experimental Section

2.1 Materials

HMX powders were synthetized in the form of particles of several hundred microns on two different chemical synthesis setups by Bachmann process[25]. Purification, crystallization in organic solvents and washing steps were also carried out, examples of which can be found in different published works[26,27] . HMX B only was further washed with an aqueous solution of mineral acid. Some particles were milled. A mixture of milled and non-milled particles was coated with an organic polymeric binder (about 5% in mass) to form a molding powder[28]. The HMX molding powder was embedded in an epoxy resin and polished mechanically (pre-polishing with SiC paper and final polishing with diamond solutions and colloidal silica) before being studied by X-ray diffraction. The molding powders were pressed uniaxially under the same conditions of pressure and temperature in the form of pellets of 1.5 mm height and 10 mm diameter and heated above 100°C to form bulk HMX compounds[28].

2.2 Tools

The X-ray diffraction instrument used was a Siemens D5000 diffractometer in θ-θ configuration with a copper anticathode and without monochromator to cut the $K\alpha_2$ radiation. A nickel filter is used to cut the Kβ radiation. The diffraction analysis range extended from 10 to 54°. The powder was deposited on a silicon surface to avoid any parasitic diffraction peak. Molding powders and pellets were glued with a stick paste onto a sample holder so that the X-ray beam was focused on the sample surface. The sample holder was rotated at 30° per minute to improve the statistics. For each sample, three diffraction patterns were recorded to evaluate the reproducibility of the experiment. A Rietveld analysis was performed on each diffraction pattern. This approach consists in calculating a theoretical diffraction pattern that best fits the experimental data. Starting from a reference structure, a refinement of the various parameters of the simulated function is performed in order to minimize the weighted profile R-factor (R_{wp}) defined by Equation (1):

$$R_{wp} = \left[\frac{\sum_i \left[w_i (I_i^{exp} - I_i^{sim})\right]^2}{\sum_i (w_i I_i^{exp})^2}\right]^{1/2} \quad \text{with } w_i = \frac{1}{\sqrt{I_i^{exp}}}$$

where I_i^{exp} is the intensity of the experimental diffraction pattern at point i along the diffraction pattern and I_i^{sim} is the intensity of the simulated diffraction pattern at point i. For details on the simulation of the diffraction pattern, see Ref.[29]. It is generally assumed that a R_{wp} ratio below 15% is acceptable for low symmetry crystals such as monoclinic HMX[29]. The I_i^{exp} peak position and shape depend on lattice parameters and structural defects. In particular, the width of the diffraction peaks contains information on the average crystallite size and the microstrain of the constituent crystals. These structural parameters can be included in the simulation profile and optimized to match the experimental pattern. For each pattern, two refinements were performed from slightly different starting parameters to evaluate the robustness of the resulting solution. The reference structures and the starting parameters I_i^{sim} used for the refinement were those determined by Choi and Boutin [4] for ß-HMX on a single crystal. Rietveld analyses were carried out with the MAUD[30] software on the whole pattern, taking Kα_1 and Kα_2 into account. It should be noted that the diffractometer contributes to both broadening and intensifying the diffraction peaks. This contribution, called the instrumental function, was independently determined with the Rietveld analysis using NIST LaB6 and silicon references. It was then implemented in MAUD and used to determine structural parameters of the crystals.

Optical microscopy images were obtained using a Keyence VHX 200 microscope.

3 Results and discussion

3.1 Synthesis and washing step

The HMX particles were synthetized on two different setups with different washing conditions giving HMX-A and HMX-B powders. The optical images and diffraction patterns of each kind of particle are different, as shown in Figure 2. The theoretical X-ray pattern of the β-HMX structure simulated from the known crystallographic parameters is also shown in Figure 2. It was used as a reference for spectral comparison of line positions and intensities.

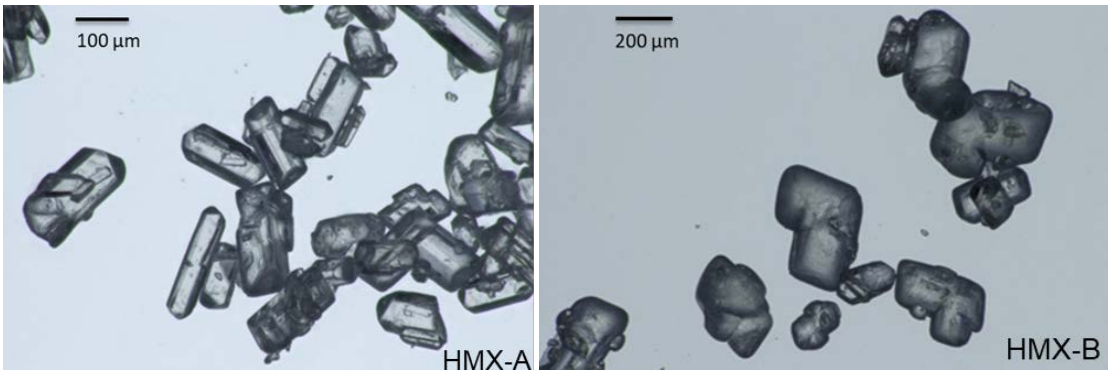

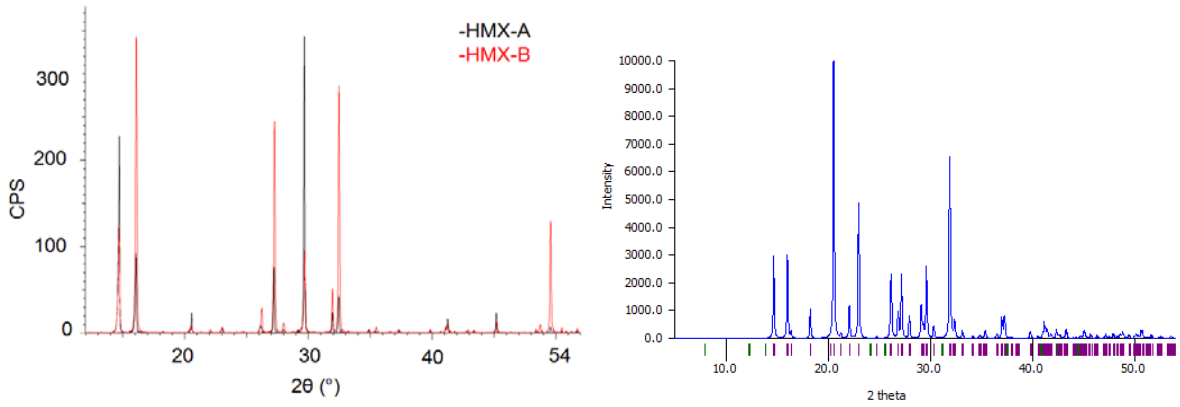

Figure 2: Optical microscope images of HMX-A (up left), HMX-B (up right) and diffraction patterns of HMX-A in black and HMX-B in red (down left) and simulation of the X-ray patterns obtained for ß-HMX (down right)

HMX-A particles have a rod type structure, while HMX-B does not exhibit any determined morphology. The patterns of HMX-A and HMX-B have neighbouring peak positions but different intensities. The peak positions and intensities of both diffraction patterns are different compared to those of the reference ß-HMX structure. Rietveld analysis were also performed from the observed diffraction pattern but no solution could be found from the other known α-HMX, δ-HMX and γ-HMX forms, nor a mixture thereof.

There are at least two possibilities to explain such differences:

It was envisioned first that crystal particles deposited on the flat surface of the holder were partially oriented along one or several crystallographic directions. Such an effect seemed realistic regarding the rod morphology of HMX-A, although it should be attenuated by rotating the sample holder. It appeared nevertheless less probable in the case of HMX-B, which exhibits no particular morphology. A Rietveld analysis was conducted and a texture component was thus added following the March-Dollase formalism where the degree of preferred orientations η (percentage of planes oriented in a given direction) is expressed versus a fitting parameter r[31,32] :

$$\eta = 100\left[\frac{(1-r)^3}{1-r^3}\right]^{1/2} \qquad \text{(equation 2)}$$

Different simulations were performed introducing a preferential orientation for different plane families, up to three for HMX-A and four for HMX-B. The agreement with experimental data was not very satisfactory as R factors lower than 25 % could not be reached in both cases. For HMX-A, the refinement gave a particularly high value of η for the (011) plane, which possibly indicated a preferential orientation along that direction (see Table 1). HMX-B on the other hand gave unrealistic results, because a R factor of 25 % could only be reached by considering preferential orientation for four planes at the same time and the total proportion of orientations largely exceeds 100 %.

(hkl)	η HMX-A (%)
(011)	39
(020)	10
(031)	22

Table 1: Percentage η of particles having a preferred orientation for HMX-A

The second possibility to explain the observed X-ray patterns is that new metastable polymorphs (new allotropic forms or hydrates) were formed after synthesis and washing. New polymorphs could be formed as pure compounds or mixed with the stable form of HMX, but as previously mentioned the X-ray patterns do not match with α-HMX, δ-HMX and γ-HMX patterns (see figure S1 to S3 in supplementary information). The hypothesis of hydrates formation is also consistent. Actually, an HMX hydrate is already known (γ-HMX)[6], among the large number of HMX solvates which has been reported, and in some cases the crystal structure has been resolved[9–12]. For comparison purpose, the patterns of HMX hydrates and solvates are also shown in supplementary information (see figure S3 to S13). This assumption is consistent with the observation by optical microscopy of two different morphologies for HMX-A and HMX-B. Moreover, polymorphism is a well-known phenomenon that has been observed many times in organic materials (energetics, therapeutics…)[1,2,6]**.** Indeed, polymorphic screening is a widely used approach that is based on the recrystallization or synthesis of the molecule in numerous solvents[1,23,24]. It is consistent with the rich polymorphism of HMX[4–8] with its six polymorphs and ten hydrates and solvates reported so far, indicating that this compound has a strong tendency to crystallize in many forms.

3.2 Milling

After milling, the HMX-A and HMX-B particles lost any particular morphology, as seen in figure 3. Their X-ray patterns were significantly changed and both closely matched the ß-HMX reference.

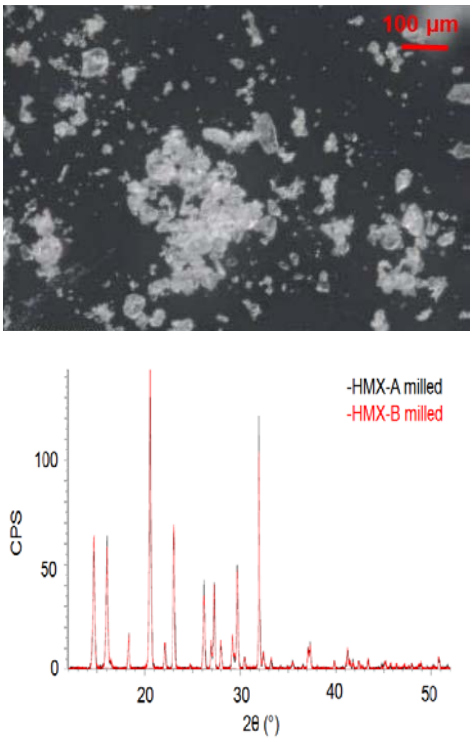

Figure 3: Optical microscope image of milled HMX (upper image), and diffraction patterns of HMX-A in black and HMX-B in red (lower image)

The structural characteristics of the milled samples determined from the Rietveld analysis are given in Table 2. The agreement between experimental and simulated patterns was considered satisfactory regarding Rwp factor values. As expected, the refined lattice parameters closely matched those of the reference structure [14]. Structural defects, i.e. crystallite size and microstrain[22] obtained for both HMX-A and HMX-B, are very close together. A direct comparison with samples before milling was not

possible because these parameters could not be determined due to the lack of reliable structural model. However, the X-ray peaks were initially narrower, indicating that structural defects were increased by milling.

Finally, the considerable modification of the X-ray patterns (mainly the relative peak intensities) after milling is certainly the most important observation that can be attributed to both the transformation of metastable polymorphs produced after synthesis into the stable ß-HMX form. The disappearance of preferential orientations is also possible.

Sample	a (A)	b (A)	c (A)	β (°)	Volume (A^3)	L (nm)	ε (%)	R_{wp} (%)
HMX-A-m	6.537 (4)	11.046 (5)	8.706 (4)	124.37 (4)	518.90 (8)	150 - 200	1.2^{-03}	13.2
HMX-B-m	6.539 (5)	11.043 (6)	8.709 (3)	124.40 (3)	518.89 (9)	150 - 200	1.3^{-03}	13.6
HMX-A-mp	6.538 (4)	11.047 (5)	8.715 (3)	124.44 (5)	519.22 (7)	100 - 120	1.1^{-03}	7.3
HMX-B-mp	6.546 (5)	11.041 (6)	8.719 (5)	124.43 (5)	519.78 (10)	100 - 120	1.1^{-03}	6.8
HMX-pr	6.547 (6)	11.057 (8)	8.718 (7)	124.45 (4)	520.52 (13)	~200	6.8^{-04}	8.7
Reference (4)	6.537	11.054	8.701	124.44	518.55	-	-	-

Table 2: Lattice parameters, cell volume, crystallite size, microstrain and R_{wp} for milled (m), molding powder (mp) and pressed (pr) HMX-A and B. Reference lattice parameters and cell volume are also given.

The transformation of metastable polymorphs into stable forms as well as an increase in structural defects after milling are quite common situations that have already been encountered in molecular materials developed for therapeutic applications[33]. Metastability could also account for the limited observation of polymorphs, hydrates, or solvates produced from ß-HMX during investigations of processing operations. This is because the commonly employed processing conditions are typically aggressive and tend to favor the formation of the stable structure of HMX. As a result, alternative structures or phases may be less frequently observed under these conditions.

3.3 Coating operation

Figure 4 displays the superimposed X-ray diffraction patterns of molding powders derived from HMX-A and HMX-B. Both patterns exhibit similarities to each other and to the previously obtained patterns from milled powders. This suggests that there are no polymorphic transformations taking place after the coating process.

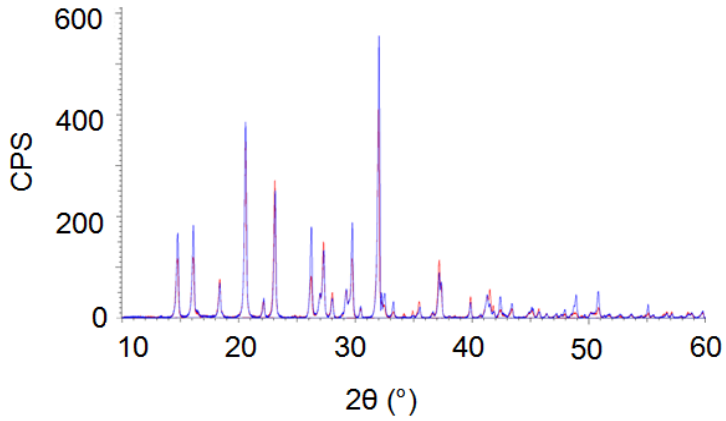

Figure 4: Diffraction patterns of HMX-A-mp (red) and HMX-B-mp (blue)

This was confirmed by Rietveld analyses as no changes are seen in terms of lattice parameters (see Table 2). However, the range of crystallite size is lowered for both samples and the observed variation is significant considering the low Rwp value. Therefore, the molding process is responsible for a further increase in structural defects in the HMX crystal.

3.4 Pressing operation

Pressed materials obtained from molding powders gave similar diffraction patterns for both HMX-A and HMX-B. The peak positions are almost unchanged and the relative intensities are only slightly modified except for the main peak which significantly increased after pressing (see Figure 5).

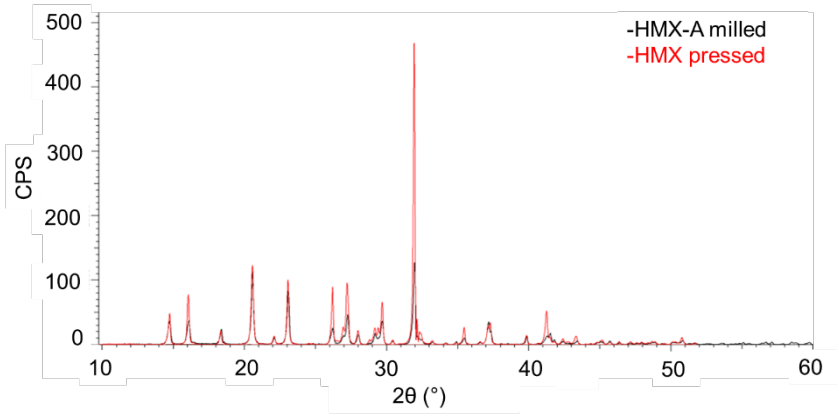

Figure 5: Diffraction patterns of milled HMX-A (black) and pressed HMX-A (red)

This very specific change can be easily explained by a preferential orientation of a given plane family, and therefore cannot be attributed to any polymorphic transformation. At the same time, a reduction in the peak linewidths was observed on pressed samples as compared with milled HMX and even more with the molding powder. Indeed, Rietveld analysis gave very similar lattice parameters but revealed an increase in crystallite size accompanied by a reduction in the concentration of microstrains on pressed samples. Both results are consistent with a loss of structural defects, which certainly result from a release of residual stresses during the heat treatment.

This situation is the opposite of what has been reported for TATB[34], where It was suggested that during pressing, sliding preserve the layered structure and the coherence in the stacking direction,

while introducing structural defects in other directions[35,36]. This refersto the anisotropic behaviour of TATB under compression[37]. Turning to HMX, the measurements made by Gao et al.[8] between 0 and 6 GPa show that the compression of the *a* axis, *b* axis and *c* axis is around 5 %. Therefore, the pressing of HMX compounds leads to an isotropic compression of the cell volume that causes less damage to the structure as compared with TATB. Moreover, the defects that are produced by the stress are more easily removed by the thermal treatments. The repairing effect of a heat treatment on the crystallographic structure is thus more efficient than the damaging effect of mechanical pressing.

4 Conclusions

The structural behaviour of HMX has been investigated at different steps of processing, from the starting powder to the bulk compounds, i.e. synthesis, milling, coating and pressing. Synthesis of HMX on two different setups with different washing conditions yields two different grain morphologies and two new diffraction patterns that differ from each other and from the initial β form. Based on Rietveld refinements, it is argued that these differences cannot result solely from preferential orientations but more probably reveal the formation of new polymorphs. After milling, the stable ß-HMX crystallographic form is obtained in both cases, indicating the metastability of the new polymorphs. Such results are comparable with numerous works reported on molecular therapeutic materials. Transposing their methodology to HMX polymorphism would be interesting but would require a structural determination with a high-resolution diffractometer or synchrotron facilities.

The observations on molding powders or pressed samples showed that β-HMX is preserved without polymorphic transformation. Rietveld refinements lead to the conclusion that the crystallite size slightly increases after the coating operation. Conversely, a significant decrease in the density of structural defects is observed after pressing. This evolution is the opposite of that observed for TATB and is probably due to the more isotropic characteristic of the crystallographic structure associated with a more efficient repairing effect of the thermal treatment.

Acknowledgements

The authors wish to thank Dr Jean-François Willart for useful discussions.

References

[1] W. C. McCrone, in *Polymorph. Chapter 8 Phys. Chem. Org. Solid State*, New-York, **1965**, pp. 725–767.

[2] H. G. Brittain, *J. Pharm. Sci.* **2012**, *101*, 464–484.

[3] H. H. Cady, A. C. Larson, D. T. Cromer, *Acta Crystallogr.* **1963**, *16*, 617–623.

[4] C. S. Choi, H. P. Boutin, *Acta Crystallogr. Sect. B* **1970**, *26*, 1235–1240.

[5] R. E. Cobbledick, R. W. H. Small, *Acta Crystallogr. Sect. B* **1974**, *30*, 1918–1922.

[6] C. P. Achuthan, C. I. Jose, *Propellants, Explos. Pyrotech.* **1990**, *15*, 271–275.

[7] P. Main, R. E. Cobbledick, R. W. H. Small, *Acta Crystallogr. Sect. C* **1985**, *41*, 1351–1354.

[8] D. Gao, J. Huang, X. Lin, D. Yang, Y. Wang, H. Zheng, *RSC Adv.* **2019**, *9*, 5825–5833.

[9] K. B. Landenberger, A. J. Matzger, *Cryst. GROWTH Des.* **2012**, *12*, 3603–3609.

[10] I. V Levakova, A. Korobko, S. Krasheninnikov, V. E. Zavodnik, *Kristallografiya* **1996**, *41*, 1015–1017.

[11] R. E. Cobbledick, R. W. H. Small, *Acta Crystallogr. Sect. B* **1975**, *31*, 2805–2808.

[12] T. M. Haller, A. L. Rheingold, T. B. Brill, *Acta Crystallogr. Sect. C* **1985**, *41*, 963–965.

[13] W. C. McCrone, *Anal. Chem.* **1950**, *22*, 954–955.

[14] C. S. Choi, E. Prince, *Acta Crystallogr. Sect. B* **1972**, *28*, 2857–2862.

[15] Z. Peralta-Inga, N. Degirmenbasi, U. Olgun, H. Gocmez, D. M. Kalyon, *J. Energ. Mater.* **2006**, *24*, 69–101.

[16] N. Degirmenbasi, Z. Peralta-Inga, U. Olgun, H. Gocmez, D. M. Kalyon, *J. Energ. Mater.* **2006**, *24*, 103–139.

[17] R. Yazici, D. Kalyon, *J. Energ. Mater.* **2005**, *23*, 43–58.

[18] N. I. Golovina, A. N. Titkov, A. V Raevskii, L. O. Atovmyan, *J. Solid State Chem.* **1994**, *113*, 229–238.

[19] Z. Xu, G. Cheng, H. Yang, X. Ju, P. Yin, J. Zhang, J. M. Shreeve, *Angew. Chemie Int. Ed.* **2017**, *56*, 5877–5881.

[20] M. Herrmann, H. Fietzek, *Powder Diffr.* **2005**, *20*, 105–108.

[21] R. B. Schwarz, C. Liu, D. G. Thompson, **2015**.

[22] G. S. Smith, R. L. Snyder, *J. Appl. Crystallogr.* **1979**, *12*, 60–65.

[23] R. J. Davey, *Cryst. Growth Des.* **2002**, *2*, 675–676.

[24] S. R. Vippagunta, H. G. Brittain, D. J. W. Grant, *Adv. Drug Deliv. Rev.* **2001**, *48*, 3–26.

[25] I. J. Solomon, L. B. Silberman, *Process for Preparing Cyclotetramethylenetetranitramine*, **1978**, 4,086,228.

[26] H. Kröber, U. Teipel, *Propellants, Explos. Pyrotech.* **2008**, *33*, 33–36.

[27] L. Wang, D. Chen, Y. Yu, H. Li, *J. Chem. Eng. Data* **2020**, *65*, 2098–2108.

[28] H. Kerviel, P. Charrue, *0 495 714 A1*, **1992**.

[29] P. Paufler, *Cryst. Res. Technol.* **1995**, *30*, 494–494.

[30] L. Lutterotti, *Nucl. Instruments Methods Phys. Res. Sect. B Beam Interact. with Mater. Atoms* **2010**, *268*, 334–340.

[31] W. A. Dollase, *J. Appl. Crystallogr.* **1986**, *19*, 267–272.

[32] E. Zolotoyabko, *J. Appl. Crystallogr.* **2013**, *46*, 1877–1879.

[33] M. Descamps, J. F. Willart, *Adv. Drug Deliv. Rev.* **2016**, *100*, 51–66.

[34] M. Guerain, A. Forzy, A. Lecardeur, H. Trumel, *Propellants, Explos. Pyrotech.* **2016**, *41*, 494–501.

[35] J. Sun, B. Kang, C. Xue, Y. Liu, Y. Xia, X. Liu, W. Zhang, *J. Energ. Mater.* **2010**, *28*, 189–201.

[36] J. R. Kolb, H. F. Rizzo, *Propellants, Explos. Pyrotech.* **1979**, *4*, 10–16.

[37] L. L. Stevens, N. Velisavljevic, D. E. Hooks, D. M. Dattelbaum, *Propellants, Explos. Pyrotech.* **2008**, *33*, 286–295.